APPLICATION OF SUCROSE AS A COSURFACTANT IN CONTROLLING THE PORE DIAMETER IN THE SYNTHESIS OF MESOPOROUS HYDROXYAPATITE NANOPARTICLES

NEGAR ABBASI AVAL*, #JAFAR JAVADPOUR*, ALIREZA BADIEI**

*Iran University of Science and Technology, School of Metallurgy and Materials Engineering, Narmak, Tehran, 16846-13114, Iran
**University of Tehran, Faculty of Chemistry, Tehran, 14155-6455, Iran

#E-mail: Javadpourj@iust.ac.ir

Submitted June 12, 2015; accepted October 19, 2015

Keywords: Mesoporous, Hydroxyapatite, Block copolymer, Sucrose, Cosurfactant

A hydrothermal approach has been employed for the synthesis of different morphologies of porous γ-AlOOH nanostructures. Mesoporous hydroxyapatite nanoparticles were synthesized using F127 Block copolymer as a soft template. For the first time, sucrose molecules were used as cosurfactant to alter the pore diameter in the mesostructured particles. Depending on the concentration of cosurfactant molecules, nanoparticles with pore diameters in the range of 50 - 96 nm were produced in this study. Furthermore, the results indicated that the use of cosurfactant molecules did not have any significant effects on the pore volume, surface area and morphology of the synthesized nanoparticles. The textural features of pore diameter, pore volume and surface area in the optimized mesoporous hydroxyapatite sample were 58 nm, 0.581 $cm^3 \cdot g^{-1}$ and 48 $m^2 \cdot g^{-1}$ respectively.
(SBA: Santa Barbara Amorphous; CTAB: Cetyl trimethylammonium bromide; HA: Hydroxyapatite; XRD: X-Ray Diffraction BET: Barrett-Emmett-Teller; BJH: Barrett-Joyner-Halenda; SEM : Scanning Electron Microscopy; FESEM: Field Emission Scanning Electron Microscopy)

INTRODUCTION

Mesoporous materials have attracted much attention due to their ordered structures, greater pore size than microporous materials and their large surface areas. These types of materials have found numerous applications in separation, catalysis and sensor technology [1]The mesoporous materials are also ideal for encapsulation of drugs, proteins and other biologically active molecules. It has been shown that small and large molecules of the drugs can be entrapped in the mesoporous materials via saturation process and released later by diffusion mechanisms [2-11]. Due to the different size of drugs and various types of the biologically active molecules, it is essential to control the size of the pores in the mesoporous materials. The use of surfactant templates is one of the methods used to control the pore size in the mesoporous particles [12]. The existing literatures mostly concentrate on the methods to increase the size of pores and there is much less published data on the pore size reduction techniques. One such report is the reduction of pore size in the synthesis of SBA with the addition of CTAB into P123 surfactant molecules. The explanation was that cationic surfactant causes the hydration of PO hydrophobic chains and the decomposition of surfactant micelles of F127 and P123 block copolymers. This means that the volume of the surfactant hydrophobic chain (PO block) was decreased by addition of the cationic surfactant and as a result, there was a reduction in the size of the pores synthesized using block copolymer [13]. Increasing the length of the carbon chains and hydrophobic volume of the surfactant can also contribute to growth of the pores. The cosurfactants may also act as swelling agents because the growth of the hydrophobic volume will dominate over the growth of the hydrophilic volume by the addition of co-surfactants [14, 15]. Due to the importance of pore size control in the mesoporous materials, the main objective in this study was to control the size of the pores of the mesoporous hydroxyapatite particles. Hydroxyapatites are similar to bones and hard tissues in composition [16-18] and are widely used in drug delivery [19-22] and bone tissue engineering [23-29] applications. Sucrose was used as the cosurfactant in this study. The idea behind using sucrose was to be able to change the pore size in the porous hydroxyapatite nanoparticles by changing the strength of the hydrogen bond between the calcium ions and block copolymer.

EXPERIMENTAL

Materials

Calcium acetate ($Ca(C_2H_3OO)_2$) with molecular weight of 158.17 g·mol^{-1} was obtained from Panreac QUIMCA Company. Potassium di-hydrogen phosphate (KH_2PO_4) was purchased from Merck Company. Pluronic, a triblock copolymer manufactured by Sigma-Aldrich with chemical formula $EO_{99}PO_{65}EO_{99}$ and molecular weight of 12,600 g·mol^{-1} was used as templating surfactant. Table Sucrose ($C_{12}H_{22}O_{11}$) was used as co-surfactant in this study. Ammonia used in this work was also obtained from Merck Company. All chemicals were used without further purification.

Synthesis of mesoporous HA in the absence of co-surfactant

3 g of F127 together with 6.32 g of calcium acetate (0.04 mol) were dissolved in 100 ml of distilled water and placed on a magnetic stirrer. The pH of the initial solution was measured to be around 7.30 and it was raised to 12 by the addition of ammonia. In a separate beaker, 3.27 g of potassium di-hydrogen phosphate was dissolved in 60 ml of distilled water (0.024 mol) and added drop wise to the initial solution. The resulting whitish solution was transferred to a reflux held at 90°C rotating at the speed of 600 rpm to be refluxed for 24 hr. The final solution was centrifuged 5 times with distilled water and each time for 4 minutes. The resulting precipitate was dried in an oven at 100°C for 24 hr. The surfactant removal was accomplished by calcination of the dried powder at 550°C for 6 hr [30]. The calcinated sample was designated as HA-1.

Synthesis of mesoporous HA in the presence of co-surfactant

The process of synthesis started by initially dissolving 3 g of F127 in 50 ml of distilled water. In a separate beaker 6.32 g of calcium acetate (0.04 mol) plus the amounts of sucrose indicated in Table 1 were dissolved in 50 ml distilled water and added to the initial solution. The pH of the mixture was increased to 12 by the addition of ammonia. Thereafter, 3.27 g of potassium di-hydrogen phosphate (0.024 mol) was dissolved in 60 ml distilled water and added drop wise to the initial solution. The rest of the procedure is similar to the previous section.

Characterization

X-ray diffraction (JEOL (Model: JDX-8030)) with Cu-Kα source, 30 kV voltage and 20 mA current was utilized for crystallographic and phase analysis of the synthesized samples. Nitrogen adsorption-desorption isotherms were collected in a BELSORP-mini II apparatus after degassing the samples at 200°C for 120 min. The specific surface areas were calculated using the Barrett-Emmett-Teller (BET), while the pore volume and pore diameters were calculated from the adsorption branches of the isotherm from the Barrett-Joyner-Halenda model (BJH). Meanwhile, scanning electron microscopy (SEM:TEscan) working at an acceleration voltage of 30 kV and field emission scanning electron microscopy (FESEM:Hitachi S4160) working at an acceleration voltage of 15 kV were used to study the morphology of the obtained powder.

RESULTS

XRD analysis was used to examine the nature of crystalline structure in the HA-1 sample (Figure 1).

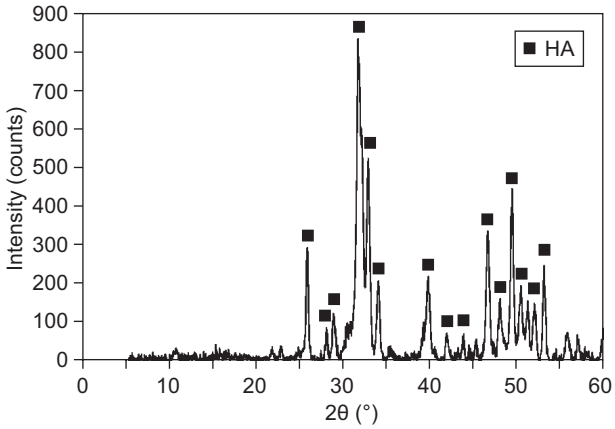

Figure 1. XRD pattern for the HA-1 sample.

Table 2. The physical characteristics of the HA-1 sample.

BET Surface area ($m^2 \cdot g^{-1}$)	Average pore diameter (nm)	Pore volume ($cm^3 \cdot g^{-1}$)
50	92	0.836

Symbol explanations: BET = specific surface area as described by the theory of Brunauer, Emmett and Teller [31], Pore diameter = pore diameter as defined by the Theory of Barrett, Joyner, Halenda [32], Pore Volume = pore volume as defined by Theory of Barrett, Joyner, Halenda [32].

Table 1. Synthesized samples with various amounts of sucrose and their corresponding codes.

Sample code	HA-2	HA-3	HA-4	HA-5
amount of sucrose (mol)	Equal to Calcium	0.004 fold Calcium	0.002 fold Calcium	0.001 fold Calcium
amount of sucrose (g)	13.68	1.37	0.68	0.3

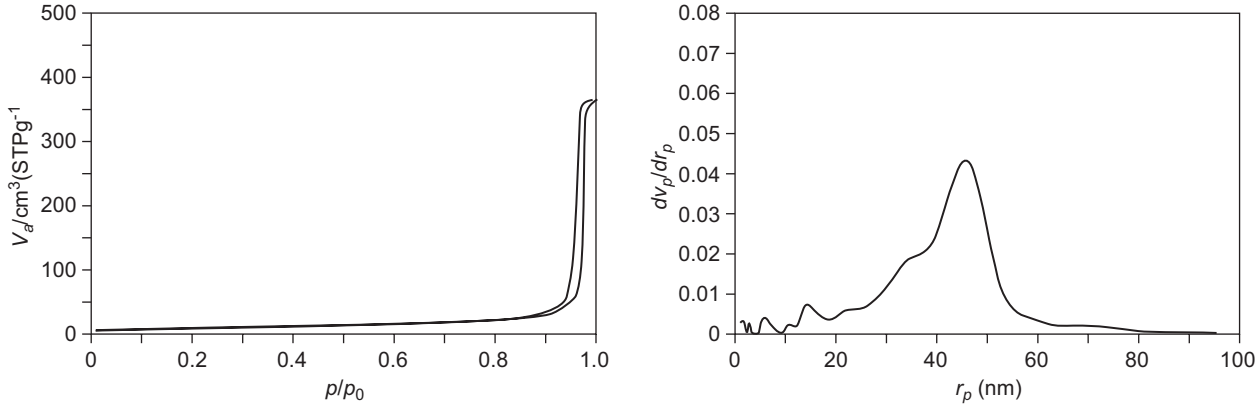

Figure 2. a) N_2 adsorption-desorption isotherms and b) BJH pore size distribution for the HA-1 sample.

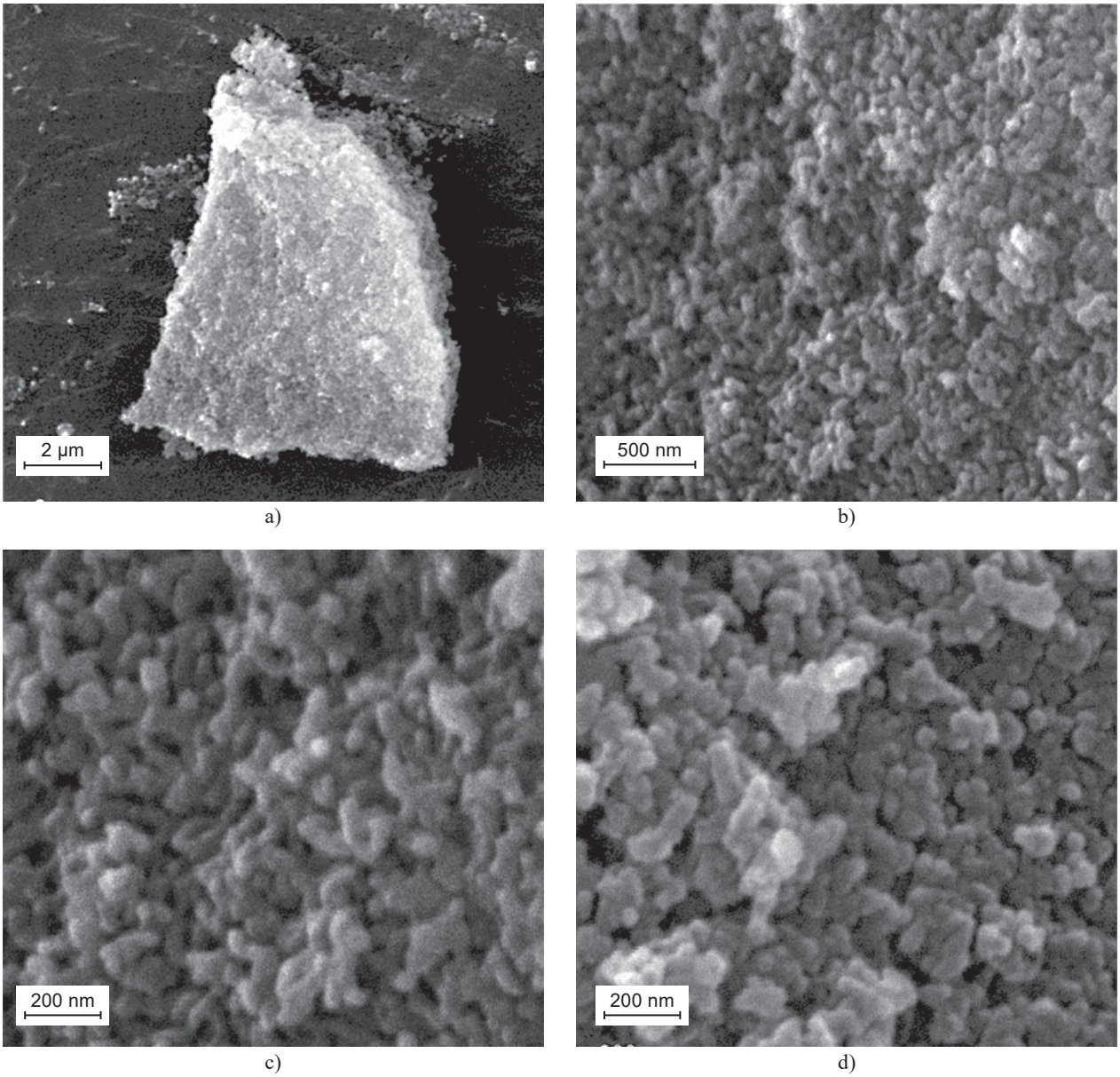

Figure 3. Scanning electron microscopy images of HA-1 sample at different magnifications.

The size distribution and surface area were extracted from BJH and BET equations, respectively. The N_2 adsorptions-desorption isotherm and size distribution data for the pores of sample HA-1 are presented in Figure 2.

The information related to size, volume of the pores and the BET surface area of HA-1 are summarized in Table 2.

The scanning electron microscope images (Figure 3) were used to study the morphological features of the synthesized powders (HA-1).

The physical characteristics of the pores in the HA-2, HA-3, HA-4 and HA-5 samples such as pore diameters, pore volume and BET surface area were also investigated using nitrogen adsorption-desorption analysis, the result of which are presented in Figure 4 and Table 3.

The HA-4 was selected as optimum sample which will be discussed later; so, the FESEM (Field Emission Scanning Electron Microscope) images were produced for just the sample HA-4 which are shown in Figure 5 .

Table 3. The physical characteristics of the pores in HA-2, HA-3, HA-4 and HA-5 samples.

	BET Surface area ($m^2 \cdot g^{-1}$)	Average pore diameter (nm)	Pore volume ($cm^3 \cdot g^{-1}$)
HA-2	5	78	0.070
HA-3	46	58	0.662
HA-4	48	58	0.581
HA-5	46	50	0.463

Symbol explanations: BET = specific surface area as described by the theory of Brunauer, Emmett and Teller [31], Pore diameter = pore diameter as defined by the Theory of Barrett, Joyner, Halenda [32], Pore Volume = pore volume as defined by Theory of Barrett, Joyner, Halenda [32].

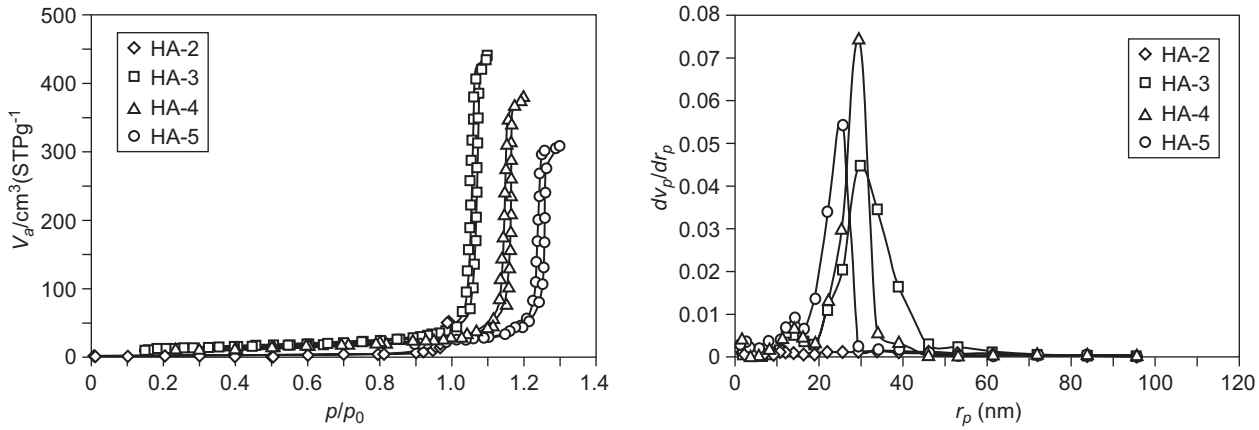

a) b)

Figure 4. a) Adsorption-desorption isotherms, and b) BJH pore size distribution data for HA-2, HA-3, HA-4 and HA-5 samples.

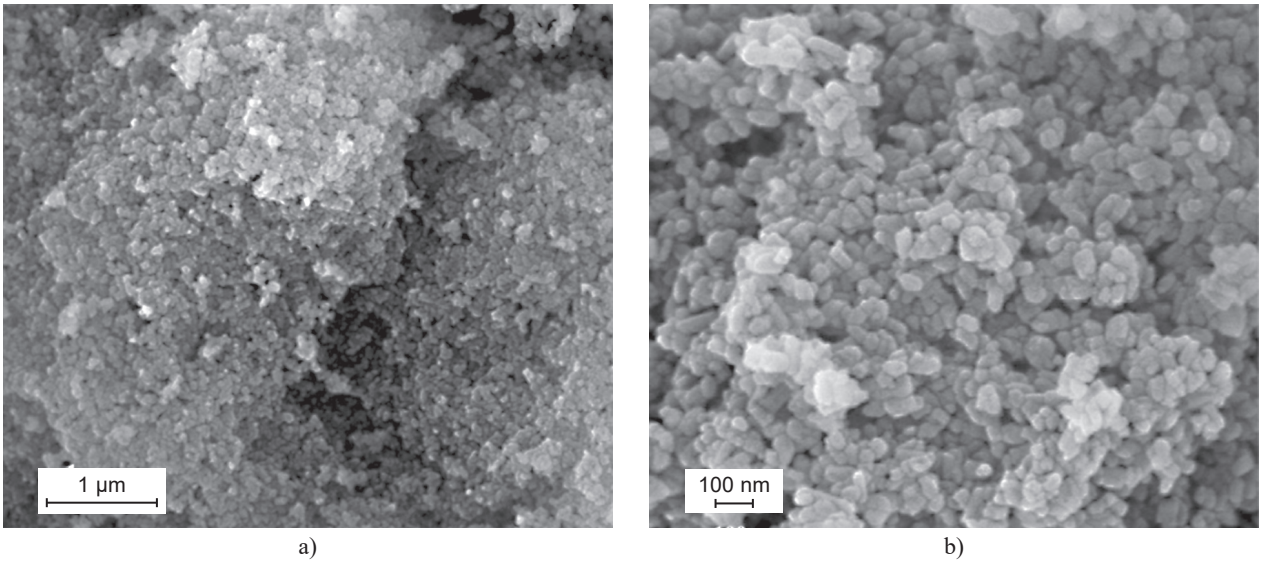

a) b)

Figure 5. Field emission scanning electron micrographs of the HA-4 sample at two different magnifications.

DISCUSSION

A comparison between the result shown in Figure 1 and standard card no.00-009-0432 for HA indicates that the detected peaks in this pattern are all associated with the standard hydroxyapatite. N_2 adsorption-desorption analysis was used to study the physical characteristics of the pores in the HA-1 sample. According to the result shown in Figure 2a, the adsorption-desorption isotherm for the sample HA-1 is that of type 5, while the hysteresis loop exhibited H1 type behavior indicating the presence of cylindrical pores with open ends [33]. The start of the adsorption process at a rather high relative pressure is an indication for the large size of the pores [33]. This point is further confirmed by the pore size distribution (BJH data) shown in Figure 2b. The readily accessible nature of the pores is illustrated by the steep slope of the adsorption-desorption diagram [33]. As indicated in Table 2, the pores are rather large in the HA-1 sample. It is thought that the large pore size is related to the weak hydrogen bonding between the calcium precursor and F127 surfactant molecules. According to the mechanism shown in Figure 6a, it can be seen that the hydrogen bonding between the calcium precursor and the surfactant molecule causes precipitation of the calcium phosphate on the micelles and the formation of this mesoporous material[30].

The calcium precursor used in the study by Y.F. Zhao *et al.* [30] was an organic- inorganic material (calcium d-pantothenate) able to establish a strong hydrogen bond between the surfactant molecule due to the presence of an organic component. Then, the calcium ions attach on the micelles and do not scatter within the hydrophilic component of the surfactant. The latter behavior appears to inhibit excessive growth of the micelles. The calcium precursor used in this research was calcium acetate. Calcium acetate is not as strong as calcium d-pantothenate inas much as it does not have organic component and then it is not capable to have a strong hydrogen bond. This point was thought to be the reason for enlargement of pore size in the HA-1 sample. In other words, this precursor was unable to establish an appropriate bond between the hydrophilic ends of the surfactant molecule and as a result some of the calcium ions did not adhere on the micelles. Instead they were randomly scattered among the hydrophilic ends leading to the opening of the micelle structure and consequently the enlargement of the pore size (see the schematic presentation shown in Figure 6b). This weakness was compensated by the use of sucrose molecules as co-surfactant in this study. Sucrose is expected to act as an intermediate to establish a hydrogen bond between the calcium precursor and the surfactant. Different amounts of sucrose molecules (see Table. 1) were used in the synthesis of the samples coded such as HA-2, HA-3, HA-4 and HA-5. The physical characteristics of the pores in the HA-2, HA-3, HA-4 and HA-5 samples such as pore diameters, pore volume and BET surface area are presented in Table 3. A look at Table 3 reveals that both surface area and volume of

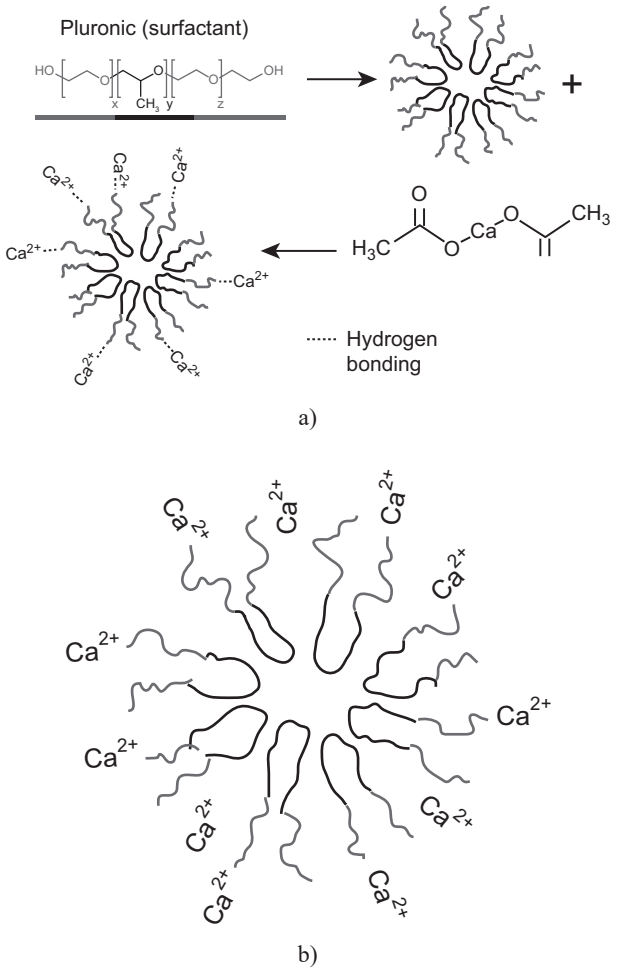

Figure 6. Bonding mechanism between calcium precursor and surfactant molecules in HA-1 sample a), and b) unbalanced distribution of calcium ions between hydrophilic heads of surfactant.

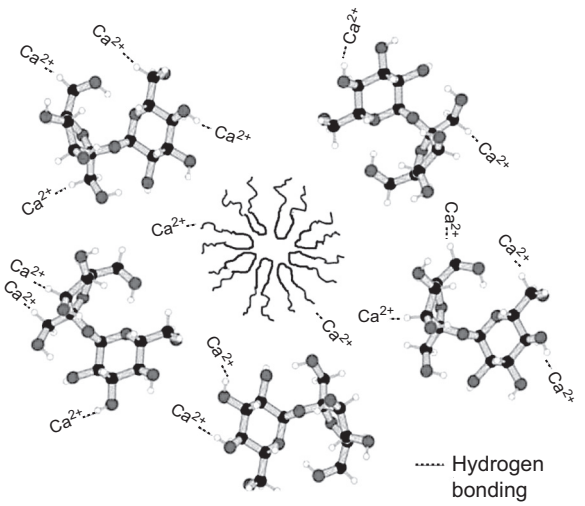

Figure 7. Schematic representation of sucrose molecule attracting calcium ions in aqueous medium.

the pores decreased significantly in the HA-2 sample compared to HA-1 sample. It seems that the amount of sucrose is much more than it was needed and the adsorption of Ca ions by the large number of sucrose molecules limited the number of bonding between the Ca ions and the surfactant molecules (a situation shown schematically in Figure 7).

In order to find the optimum sucrose content for the reinforcement of hydrogen bonding, lower amounts (Table 1.) were used in the synthesis of HA-3, HA-4 and HA-5 samples. As it is indicated in Figure 4, adsorption of nitrogen in all samples started at a same relative pressure and ends at a same relative pressure too. Slope in the adsorption- desorption diagrams followed similar trend in all three samples. The adsorption-desorption isotherms were of type 5, with the hysteresis loop of type H1. As mentioned before, this type of hysteresis loop is an indication for cylindrical pores with open endse [33].

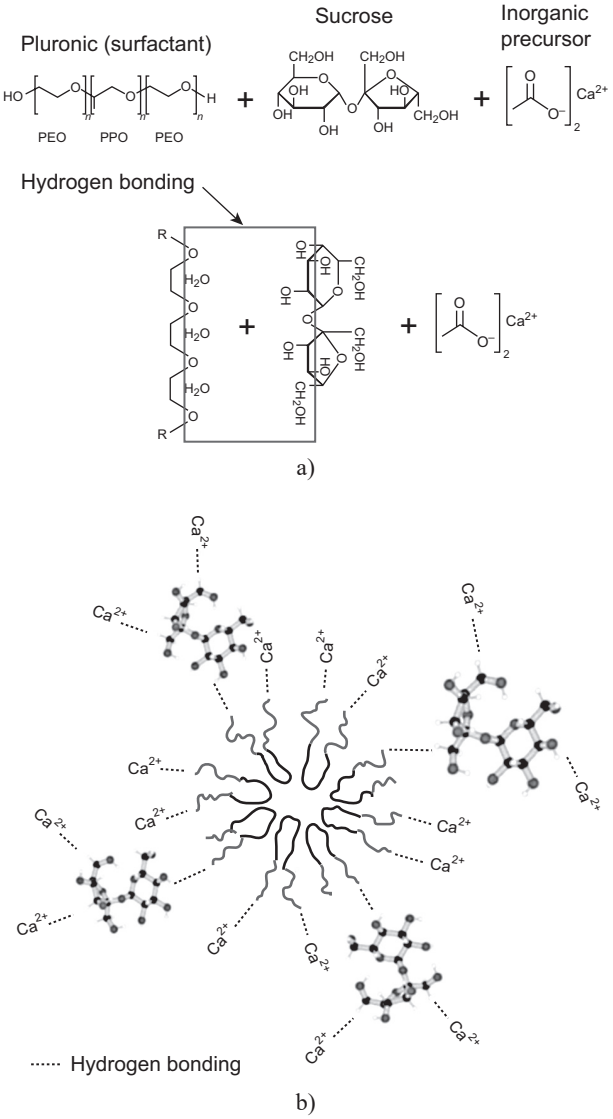

Figure 8. Schematic representation of sucrose molecules function as co-surfactant.

Therefore, the addition of the sucrose co-surfactant had no effect on morphology of the pores. However, there was a significant difference between the volumes of gas adsorbed by the pores (0.463 - 0.662 $cm^3 \cdot g^{-1}$). The pore size distribution in these three samples (BJH diagrams) and their corresponding BET surface areas, pore volume and average pore diameters are presented in Figure 4, and Table 3. The data presented in Table 3, verifies the proposed theory about the role of sucrose as the co-surfactant and its reinforcing effect on the hydrogen bonding between the calcium precursor and the surfactant molecules (Figure 8). The sucrose molecules have acted as source of OH functional groups and thus have been able to compensate the deficiency of hydrogen bondings. This process reduces the number of free Ca ions within hydrophilic ends of the surfactant molecules and therefor brings about a reduction in the pore diameter.

A comparison between the pore size distribution data shows that the pore size uniformity is highest in the HA-4 with 0.68 g of the sucrose content. The average pore radius in this sample is about 29 nm (Figure 4). This pore size of radius has occupied most of the volume of adsorbed gas in the sample. Furthermore, in the HA-3 sample similar to the HA-4 sample, average radius of the pores is about 29 nm, though a smaller volume has been occupied by this size of the pores as compared to the HA-4 samples (Figure 4). In the HA-5 sample, the average radius of the pores is something about 25 according to the diagram, but only a small volume of gas is occupied by pores of this size in this sample. Comparison of the SEM micrographs of HA-1 and HA-4 samples in Figures 3 and 5 shows that the addition of sucrose as co-surfactant has almost no effect on morphology of the nanoparticles and it merely reduced the size of pores in the HA-4 sample.

CONCLUSIONS

A novel technique to control the pore diameters of porous hydroxyapatite nanoparticles was implemented in this paper. It was demonstrated that the use of sucrose molecules as cosurfactant was effective in producing mesoporous nanoparticles with properties that can be tailor-made according to the specific application. A mechanism was proposed for the role of sucrose molecules as cosurfactant in the synthesis process adopted in this study.

REFERENCES

1. Ariga K., Vinu A., Hill J. P., Mori T.: Coordination Chemistry Reviews *251*, 2562 (2007).
2. Vallet-Regí M., Balas F., Colilla M., Manzano M.: Progress in Solid State Chemistry *36*, 163 (2008).
3. He Q., Zhang J., Chen F., Guo L., Zhu Z., Shi J.: Biomaterials *31*, 7785 (2010).

4. Vallet-Regi M., Ramila A., Del Real R., Pérez-Pariente J.: Chemistry of Materials *13*, 308 (2001).
5. Shi X., Wang Y., Ren L., Zhao N., Gong Y., Wang D.-A.: Acta biomaterialia *5*, 1697 (2009).
6. Signoretto M., Ghedini E., Nichele V., Pinna F., Crocellà V., Cerrato G.: icroporous and Mesoporous Materials *139*, 189 (2011).
7. Vallet-Regí M.: Chemistry-A European Journal *12*, 5934 (2006).
8. Vallet-Regí M., Ruiz-Hernández E.: Advanced Materials *23*, 5177 (2011).
9. Wang S.: Microporous and mesoporous materials *117*, 1 (2009).
10. Zhang C., Li C., Huang S., Hou Z., Cheng Z., Yang P., Peng C., Lin J.: Biomaterials *31*, 3374 (2010).
11. Zhu Y., Kaskel S.: Microporous and Mesoporous Materials *118*, 176 (2009).
12. Vallet-Regí M., Balas F., Colilla M., Manzano M.: Solid State Sciences *9*, 768 (2007).
13. Zhang W.-H., Zhang L., Xiu J., Shen Z., Li Y., Ying P., Li C.: Microporous and mesoporous materials *89*, 179 (2006).
14. Feng P., Bu X., Pine D. J.: Langmuir *16*, 5304 (2000).
15. Wang Y., Zhu S., Mai Y., Zhou Y., Zhu X., Yan D.: Microporous and Mesoporous Materials *114*, 222 (2008).
16. Best S., Porter A., Thian E., Huang J.: Journal of the European Ceramic Society *28*, 1319 (2008).
17. Kalita S. J., Bhardwaj A., Bhatt H. A.: Materials Science and Engineering: C *27*, 441 (2007).
18. Vallet-Regí M.: Comptes Rendus Chimie *13*, 174 (2010).
19. Fan J., Lei J., Yu C., Tu B., Zhao D.: Materials chemistry and physics *103*, 489 (2007).
20. Guo Y.-P., Yao Y.-B., Guo Y.-J., Ning C.-Q.: Microporous and Mesoporous Materials *155*, 245 (2012).
21. Verron E., Khairoun I., Guicheux J., Bouler J.-M.: Drug discovery today *15*, 547 (2010).
22. Yang P., Quan Z., Li C., Kang X., Lian H., Lin J.: Biomaterials *29*, 4341 (2008).
23. Bose S., Tarafder S.: Acta biomaterialia *8*, 1401 (2012).
24. Jiang D., Zhang J.: Current Applied Physics *9*, S252 (2009).
25. Prae-ravee K., Kuanchertchoo N., Wetprasit N., Supaphol P.: Materials Science and Engineering: C *32*, 758 (2012).
26. Vallet-Regi M., González-Calbet J. M.: Progress in Solid State Chemistry *32*, 1 (2004).
27. Rezwan K., Chen Q., Blaker J., Boccaccini A. R.: Biomaterials *27*, 3413 (2006).
28. Zhang J., Liu G., Wu Q., Zuo J., Qin Y., Wang J.: Journal of Bionic Engineering *9*, 243 (2012).
29. Zhou H., Lee J.: Acta Biomaterialia *7*, 2769 (2011).
30. Zhao Y., Ma J.: Microporous and Mesoporous Materials *87*, 110 (2005).
31. Fagerlund G.: Matériaux et Construction *6*, 239 (1973).
32. Barrett E. P., Joyner L. G., Halenda P. P.: Journal of the American Chemical society *73*, 373 (1951).
33. Horikawa T., Do D., Nicholson D.: Advances in colloid and interface science *169*, 40 (2011).